Surface Composition of a Series of Dimethylsiloxane–Urea–Urethane Segmented Copolymers Studied by Electron Spectroscopy for Chemical Analysis

Xin Chen and Joseph A. Gardella, Jr.

Department of Chemistry, State University of New York at Buffalo, Buffalo, New York 14214

Tai Ho

Department of Chemistry, George Mason University, Fairfax, Virginia 22030-4444

Kenneth J. Wynne*

Chemistry Division, Office of Naval Research, Arlington, Virginia 22217-5000, and Materials Chemistry Branch, Naval Research Laboratory, Washington, D.C. 20375-5320

Received March 10, 1994; Revised Manuscript Received November 8, 1994®

ABSTRACT: Surface composition of a series of segmented poly(siloxane–urea–urethane)s have been determined by angle- and energy-dependent ESCA. The polymers are based on aminopropyl end-capped dimethylsiloxane oligomers, isophorone diisocyanate, and 1,4-benzenedimethanol. Effects of segmental length and annealing on the surface composition were investigated. It was found that when the average molecular weight of the siloxane segments reaches 27K, the topmost surface region (within 18 Å of the free surface) of a film cast from tetrahydrofuran solution is nearly pure siloxane phase. To achieve a comparable degree of surface phase concentration in films of copolymers with a siloxane segmental molecular weight of 10K, annealing at 120 °C for 15 min was required. Depth profiles based on these data showed that in as-cast films a siloxane deficient (hard-block enriched) phase several nanometers thick occurs beneath the siloxane surface layer. Annealing increases the thickness of both the siloxane-enriched and the siloxane-deficient regions.

Introduction

We are interested in multicomponent polymers and the thermodynamic and kinetic effects which influence the nature of the polymer surfaces. Our goal is to discern the compositional and morphological features relevant to the formation of minimally adhesive surfaces which inhibit the settlement of marine organisms.[1]

We have previously reported the synthesis and characterization of polyurethanes based on a series of fluorinated diols and hexamethylene diisocyanate.[2] Analysis of contact angle and angle-resolved electron spectroscopy data[3] revealed that surface composition and properties were identical to those in the bulk. To achieve surface phase separation of the low surface energy polymer component, longer chain length diols containing low surface energy segments were sought. In a continuation of that work and with the dual criteria of creating surfaces with low surface energy and low T_g to minimize mechanical locking of a prospective adherent, we have prepared and characterized a series of segmented copolymers based on aminopropyl end-capped dimethylsiloxane oligomers and isophorone diisocyanate (IPDI) with 1,4-benzenedimethanol (BDM) as the chain extender and investigated the effects of chain extenders on material properties.[4]

Surface composition and morphology of block copolymers containing poly(dimethylsiloxane) (PDMS) segments have been previously studied using angle-dependent electron spectroscopy for chemical analysis (ESCA), cross-sectional transmission electron microscopy (TEM), and attenuated total reflectance Fourier transform infrared spectroscopy (ATR-FTIR). The scope of materials investigated includes PDMS–polysulfone,[5] PDMS–poly(methyl methacrylate),[6] PDMS–nylon-6,[7] poly(α-methylstyrene)–PDMS,[8] (Bisphenol A polycarbonate)–PDMS,[9–11] and polystyrene–PDMS[12–14] of various block architectures and overall compositions. Enrichment of PDMS segments in the surface region was detected in each case due to the lower surface energy of the PDMS component in these block copolymers.

This work builds on the observation that surface composition of multicomponent polymers depends on not only their structure but also sample history. It was shown that surface composition of solution cast films of block copolymers can be changed by either using selective solvents[7,15] or by annealing.[7,8,11,16]

We are interested in the region within 100 Å of the air–polymer interface, and ESCA has been established as an effective tool to probe this region. However, photoelectron intensities detected by ESCA are convoluted signals, i.e. all atoms within the path of the probing X-ray contribute to the signal but the contribution of each decreases exponentially with the distance from the free surface.[17] The convoluted nature of the signal distorts depth profiles for samples with compositional gradients. To recover the depth profiles for such samples, a deconvolution procedure must be applied to the ESCA data.

Several research groups have addressed this problem of deconvolution. The methods developed generally involve introducing additional constraints to the equations describing the convoluted signals. These equations can be solved by numeric methods,[18] by inverse Laplace transform,[19,20] or by the method of regularization.[21–23] In this paper we show that, with the constraints generally adopted in the deconvolution process, depth profiles of the individual segments in a

® Abstract published in *Advance ACS Abstracts,* February 1, 1995.

0024-9297/95/2228-1635$09.00/0

Table 1. Molecular Weights of the Segmented Copolymers

no.	sample ID	PDMS MW[a]	reacn stoichiometry PDMS:IPDI:BDM	copolymer MW[b] M_w	M_n	M_w/M_n
1	PDMS1K-IP-B0	1000	1:1:0	16 700	12 000	1.4
2	PDMS1K-IP-B0.5	1000	2:3:1	17 600	11 800	1.5
3	PDMS2.4K-IP-B0	2400	1:1:0	65 000	30 700	2.1
4	PDMS2.4K-IP-B1	2400	1:2:1	76 500	27 700	2.8
5	PDMS2.4K-IP-B2	2400	1:3:2	42 700	19 100	2.2
6	PDMS10K-IP-B0	10000	1:1:0	109 000	54 500	2.0
7	PDMS10K-IP-B2	10000	1:3:2	81 200	29 200	2.8
8	PDMS27K-IP-B2	27000	1:3:2	198 000	149 000	1.3

[a] Amino-terminated siloxane oligomers with molecular weight provided by the supplier. [b] Polymer molecular weight determined by GPC.

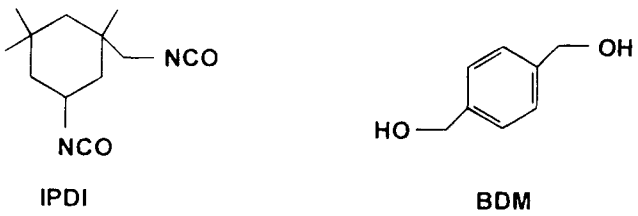

$H_2N(CH_2)_3$-[$Si(CH_3)_2$-O]$_n$-$Si(CH_3)_2$-$(CH_2)_3NH_2$

PDMS Oligomer

-[-PDMS-[(IPDI)$_m$-(BDM)$_{m-1}$]-]$_p$-

PDMS-PU Segmented Copolymer

Figure 1. Structure of PDMS–PU segmented copolymers.

segmented copolymer can be reconstructed from ESCA data by numerical methods. Ratner and co-workers have solved a similar problem by the method of regularization.[22]

Experimental Section

A series of segmented copolymers based on aminopropyl end-capped dimethylsiloxane oligomers (PDMS) and isophorone diisocyanate (IPDI) with 1,4-benzenedimethanol (BDM) as the chain extender was prepared with a two-step polymerization. First, reaction between IPDI and BDM was carried out in bulk at elevated temperatures without catalyst. In the second stage, the reaction between PDMS oligomers and diisocyanate intermediates was carried out in tetrahydrofuran (THF) solution at room temperature. Details of the synthetic procedure have been described in a separate publication.[4] The structure of these polymers is shown in Figure 1, and molecular weight data are listed in Table 1. Nomenclature for the copolymers is as follows, illustrated for PDMS27K-IP-B2, where PDMS27K identifies the average molecular weight of the soft segment, IP the diisocyanate (IPDI), and B the chain extender (BDM) and 2 is the molar ratio of the chain extender to the siloxane oligomer. The copolymers are also designated as PDMS–PU copolymers.

Before the preparation of the films, the copolymers were soaked in an excess amount of hexane for 1 day, to remove unreacted siloxane oligomers. The copolymers were then removed from the solvent and dried in a vacuum oven at 50 °C overnight. The dried copolymers were dissolved in THF to make 0.5–1% solutions. The polymer solutions were cast into clean aluminum weighing pans and then allowed to dry in air. The films were further dried in a vacuum oven at ambient temperature for over 2 days to obtain "as-cast" films. Using the solution concentration and volume, the thickness of the films was estimated at ~50 μm. Film annealing was accomplished by heating in a vacuum oven at 120 °C for 15 min (short annealing) or 2 h (long annealing). The annealing temperature was chosen to be about 25 deg above the highest transition temperature (about 100 °C) detected by dynamic mechanical analysis.[4] No other treatment was applied to the polymer films before analysis.

Angle-dependent ESCA experiments were performed on a Perkin-Elmer Physical Electronic Model 5300 ESCA with a hemispherical analyzer and a single channel detector. The ESCA spectrometer was equipped with both Mg Kα and Ti Kα X-ray sources, and each was operated at 300 W (15 kV and 20 mA). The base pressure was maintained at lower than 10^{-8} Torr. A pass energy of 35.75 eV was chosen for all high-resolution angle-dependent acquisitions. Four takeoff angles, at 10, 15, 30, and 90°, were used with the Mg Kα X-ray source, while a single takeoff angle at 90° was used for Ti X-ray ESCA acquisitions. The takeoff angle is defined such that the direction normal to the surface of the material is 90°.

The number of measurements using the Ti Kα X-ray source was reduced to prevent radiation degradation of the samples, since the kinetic energy of the Ti Kα X-ray (4510.9 eV) is much higher than that of the Mg Kα X-ray (1253.6 eV) and the acquisition time is longer to compensate for a lower Ti X-ray intensity.[24] The sampling depth, d_s, was calculated from equation $d_s = 3\lambda \sin\theta$, where λ is the escape depth of the photoelectrons and θ is the takeoff angle. The escape depth can be estimated from empirical equations that correlate this quantity with the kinetic energy of the photoelectrons.[8,25]

Films of nylon-6 (atomic ratio of N to C is 1/6) and poly(γ-benzyl glutamate) (atomic ratio of N to C is 1/12) were used to calibrate the atomic sensitivity factor ratio of nitrogen to carbon under the same ESCA experimental conditions applied to the copolymer samples. In order to check the surface purity of these films for use as standards the elemental composition was shown to be equivalent within 3% relative standard deviation to that calculated from the Physical Electronics sensitivity factors for the instrument.[26] Secondly, curve fitting of the carbon 1s chemical states yielded predicted values for nylon-6 (e.g. 5:1 ratio between CH_x and C=O) and poly(γ-benzyl glutamate) (e.g. 8:2:2 ratio for CH_x:(C–N + C–O):(C=O).

For quantification of the ESCA signals in carbon 1s, nitrogen 1s, silicon 2p, and oxygen 1s regions, spectra were recorded at high-resolution conditions. ESCA peak areas were measured by a Perkin-Elmer 7500 computer with the PHI ESCA version 2.0 software. An average of three independent runs was taken for all ESCA measurements.

Calculations. For convenience, the PDMS–PU segmented copolymer chains are divided into soft and hard segments. A soft segment is an oligomeric siloxane with the two $-NH_2$ end group moieties excluded, since the $-NH_2$ groups become part of the urea groups after polymerization. A hard segment consists of the two urea groups from reactions between IPDI and the siloxane oligomers and the moieties of IPDI and BDM. The average number of IPDI and BDM moieties in a given hard segment depends on the reaction stoichiometry. For example, the hard segment of sample 5 (Table 1) is composed of 2 $-NH_2$, 3 IPDI, and 2 BDM groups. The soft segment for this sample is a siloxane oligomer of 30 repeat units (MW = 2400).

The relationship between the weight percentage of PDMS (X) and the ratio of nitrogen atoms to carbon atoms, N/C, measured by ESCA is expressed by eqs (1–6). Here, n is the

$$\frac{N}{C} = \frac{[(100 - X)/(MW_{hard})](\#^{N}_{hard})}{[(100 - X)/(MW_{hard})](\#^{C}_{hard}) + [X/MW_{soft}](\#^{C}_{soft})} \quad (1)$$

$$MW_{hard} = 222\#^{IPDI} + 138\#^{BDM} + 32 \quad (2)$$

$$MW_{soft} = 74n + 142 \quad (3)$$

$$\#^{N}_{hard} = 2\#^{IPDI} + 2 \quad (4)$$

$$\#^{C}_{hard} = 12\#^{IPDI} + 8\#^{BDM} \quad (5)$$

$$\#^{C}_{soft} = 2(n + 1) + 6 \quad (6)$$

number of repeat units in each siloxane oligomer, $\#^{IPDI}$ and $\#^{BDM}$ are the numbers of IPDI and BDM, respectively, in a hard segment. The numbers of carbon atoms in a hard segment and a soft segment are $\#^{C}_{hard}$ and $\#^{C}_{soft}$. Nitrogen atoms only exist in the hard segments, and each hard segment contains $\#^{N}_{hard}$ nitrogen atoms. The molecular weight of a hard segment is MW_{hard} and the molecular weight of a soft segment is MW_{soft}.

The ratio of N/C, instead of Si/C, is chosen to calculate the PDMS surface concentrations because of the larger variation in nitrogen concentration at different sampling depths. This results in higher sensitivity in PDMS wt % calculations. Concentrations were also calculated from Si/C ratios for a selected set of samples. The resultant concentration data fell within error limits as equivalent to that calculated from N/C ratios.

Recovery of the Depth Profile from ESCA Data. The intensities of the photoelectronic response from nitrogen and carbon atoms as functions of the takeoff angle can be formulated in the derivative form. They are

$$dI_N(\theta) = F\alpha_N N_N(x) K e^{-x/(\lambda_N \sin\theta)}\, dx \quad (7)$$

$$dI_C(\theta) = F\alpha_C N_C(x) K e^{-x/(\lambda_C \sin\theta)}\, dx \quad (8)$$

where I is the detected intensity of photoelectrons from a given atom, subscripts N and C denote nitrogen and carbon, respectively, θ is the takeoff angle, F is the X-ray flux, α is the cross-section of photoionization in a given shell of a given atom for a given X-ray energy, $N(x)$ is the depth profile of the atomic density, x is the vertical distance from the free surface, K is a spectrometer factor, and λ is the escape depth of the electrons.[17]

If one further assumes F, K, and α are independent of x and define normalized intensity $I'(\theta)$ as $I(\theta)/(F\alpha K)$. By integration, eqs 7 and 8 give

$$I_N'(\theta) = I_N(\theta)/(F\alpha_N K) = \int_0^\infty N_N(x) e^{-x/(\lambda_N \sin\theta)}\, dx \quad (9)$$

$$I_C'(\theta) = I_C(\theta)/(F\alpha_C K) = \int_0^\infty N_C(x) e^{-x/(\lambda_C \sin\theta)}\, dx \quad (10)$$

Normalized intensities for different atoms at a takeoff angle θ, usually reported as a ratio, such as I_N'/I_C', can be obtained from the ESCA spectrum.

Atomic Density Profiles. Surface atomic density profiles for nitrogen and carbon in the segmented copolymers were obtained with the following procedures. The polymer chains were first divided into soft and hard segments as described above. The number densities of carbon atoms in each type of segment were calculated to be from 25.8 to 28.7 mol/L for the soft segments, 45.5 mol/L for non-chain-extended hard segments, and from 52.5 to 54.3 mol/L for chain-extended hard segments. To calculate the atomic densities in the copolymer, it was assumed that changes in density throughout the film (<5%) and the difference between weight fraction and volume fraction values (<3%) are negligible. Thus, if $v(x)$ is the depth profile of the hard segments, atomic depth profiles for carbon and nitrogen are

$$N_C(x) = \eta v + \sigma(1 - v) \quad (11)$$

$$N_N(x) = \eta v \gamma \quad (12)$$

where η and σ are respectively the carbon densities for the hard segment and the soft segment and γ is the nitrogen to carbon ratio in the hard segment.

The depth profiles described by eqs 11 and 12 are inserted into eqs 9 and 10. The ratio of the detected intensities of photoelectrons from carbon and nitrogen, now designated as R, can be calculated and compared with experimental values.

Recovery of the Depth Profile. To facilitate the calculation, it was further assumed that photoelectrons from carbon and nitrogen atoms have the same escape depth λ. This enabled us to express the depth profile in terms of a normalized length l, which is defined as the distance from the free surface, x, divided by the electron escape depth, λ. Depth profiles of the volume fraction of the hard segment, $v(x)$, were approximated by both discrete and continuous models.

Besides expediting the calculation, the above described assumption is also justified by the following consideration. The escape depths in polymers for photoelectrons are not known precisely; in practice, an estimation can be obtained using a correlation suggested by Seah and Dench.[25] By that correlation it was calculated that escape depths for C 1s and N 1s photoelectrons are 34 and 32 Å, respectively. There is a considerable degree of uncertainty associated with these numbers, as the data used to derive the correlation scatter significantly.[25] On the other hand, by comparison of the kinetic energies of the photoelectrons it is certain that the difference between λ_C and λ_N is less than 10%. An assumption of λ_C equal to λ_N is warranted because the information used as the basis is reliable. The effects of different assumptions on the ratio between λ_C and λ_N on the shape of the deconvoluted concentration depth profile will be discussed in a later section.

Discrete Model. In the discrete model, $v(x)$ is approximated as the sum of nine step functions. Each step function staggers the previous one by a distance varying from 0.1λ to 0.85λ determined by trial and error. The integrations described by eqs 9 and 10 were carried out numerically, each as the summation of a sequence of numerical values. The upper limit for the integration was 5λ, and the increment was $\lambda/100$. By continual adjustment of the heights of the constituent step functions, a depth profile was obtained that gives photoelectronic responses consistent with ESCA results for each copolymer.

Continuous Model. In fitting the experimental data with the discrete model, it was revealed that $v(x)$, instead of monotonically increasing with x, has a maximum. This finding was used to guide the selection of a continuous function to describe $v(x)$. We used a four-parameter compound Gaussian distribution model of the form

$$y(l) = y_1 \exp[-0.5(l - l_1)^2/\sigma_1^2] \quad l \le l_1$$
$$= 1 + (y_1 - 1)\exp[-0.5(l - l_1)^2/\sigma_2^2] \quad l > l_1 \quad (13)$$

where $y = v(l)/v(\infty)$, $v(\infty)$ is the bulk value of v; y_1, a parameter, is the y value at the maximum of the profile; l is the distance from the surface divided by the escape depth; l_1, a parameter, is the location of the maximum of the profile; σ_1, a parameter, characterizes the shape of the profile to the left of the maximum; and σ_2, a parameter, characterizes the shape of the profile to the right of the maximum.

Optimal values for the parameters were determined by minimizing the objective function ψ defined as

$$\psi = \{1/n \sum^{n} \{[R_{calc}(y_1, l_1, \sigma_1, \sigma_2, \theta_n) - R_{exp}(\theta_n)]/R_{exp}(\theta_n)\}^2\}^{1/2} \quad (14)$$

Table 2. PDMS Weight Percent of the As-Cast Samples from THF Solutions

no.	sample ID	PDMS wt % $\theta = 10°$	$\theta = 15°$	$\theta = 30°$	$\theta = 90°$	bulk
1	PDMS1K-IP-B0	93.6 ± 1.3	90.6 ± 2.3	86.8 ± 2.2	83.5 ± 1.3	79.0
2	PDMS1K-IP-B0.5	88.6 ± 2.3	83.9 ± 0.4	77.2 ± 1.2	71.4 ± 1.0	68.8
3	PDMS2.4K-IP-B0	96.8 ± 0.8	94.4 ± 1.0	92.4 ± 0.2	90.6 ± 0.3	90.3
4	PDMS2.4K-IP-B1	95.0 ± 2.7	92.1 ± 1.4	83.9 ± 1.8	79.4 ± 1.6	79.4
5	PDMS2.4K-IP-B2	88.0 ± 1.8	84.9 ± 1.6	78.5 ± 1.5	72.5 ± 0.9	70.8
6	PDMS10K-IP-B0	98.9 ± 0.7	98.5 ± 0.5	97.7 ± 0.1	97.0 ± 0.6	97.5
7	PDMS10K-IP-B2	97.7 ± 0.5	97.0 ± 1.4	93.5 ± 1.0	90.0 ± 1.5	91.1
8	PDMS27K-IP-B2	100 ± 0.0	99.1 ± 0.9	98.0 ± 0.7	97.2 ± 1.3	96.5

where n is the number of takeoff angles. The optimization was achieved using the Gauss–Newton method.[27] The starting values for the optimization procedures were obtained by scanning the five-dimensional space. In the latter, a grid was imposed on the $(y_1,l_1,\sigma_1,\sigma_2)$ space, ψ values at selected intersections were calculated, and the coordinates of the location where the minimum was found were used as the starting values.

In principle, one should be able to find the absolute minimum for the objective function ψ with a sequence of screening and optimization procedures as described above. The following factors lead to uncertainties associated with the resulting parameters. The larger the uncertainties of the experimental data, the larger the uncertainties of the optimized results. Larger coverage of the grid and shorter distances between the intersections on the grid would reduce uncertainties of the results. In this work, the calculated atomic ratios between carbon and nitrogen based on the optimized parameters usually agree with the ESCA data within the experimental uncertainties.

Results and Discussion

Surface Composition of PDMS–PU Films by ESCA. Structural Effects. The measured PDMS surface concentrations of the PDMS–PU segmented copolymer films cast from THF in air are summarized in Table 2. The surface concentrations of PDMS in all samples are higher than the bulk values. PDMS surface phase separation can be attributed to the lower surface energy of the PDMS segments at the polymer–air interface as compared with that of the polar hard segments.[28] ESCA results for the PDMS–PU segmented copolymers are angle-dependent, indicating a gradient in concentration of PDMS over the surface region.

The average soft and hard segmental lengths are found to have significant effects on the surface composition. Concentrations of PDMS in the surface region of the as-cast films of polymers PDMS1K-IP-B0, PDMS2.4K-IP-B0, and PDMS10K-IP-B0 are listed in Table 2. There is no chain extender in the hard segments of these three copolymers, and the average molecular weights of the PDMS segments are 1K, 2.4K, and 10K. In this series, polymer PDMS10K-IP-B0 shows the highest PDMS surface concentration at every takeoff angle.

Surface compositions of the as-cast films of three copolymers PDMS2.4K-IP-B2, PDMS10K-IP-B2, and PDMS27K-IP-B2 are also listed in Table 2. Each hard segment of these copolymers contains on average two BDM moieties, and the average molecular weights for the soft segments are 2.4K, 10K, and 27K, respectively. Again, the sample with the highest average molecular weight for the soft segments has the highest PDMS surface concentration.

Data shown in Table 2 also illustrate the change in PDMS surface concentration with an increase in the length of the hard segment. In the group of PDMS–PU samples, PDMS2.4K-IP-B0, PDMS2.4K-IP-B1, and PDMS2.4K-IP-B2, the average molecular weights for the soft segments are the same, but the average lengths for the hard segment are different. It appears that the surface concentration of PDMS decreases as the length of the hard segment increases. Comparison can also be made for samples with similar *bulk* PDMS concentrations. For such samples, the length ratios of PDMS segment to hard segment are similar. Copolymers PDMS2.4K-IP-B0 and PDMS10K-IP-B2 have similar bulk concentrations of PDMS (90.3% and 91.1%). Results for these two copolymers can be found in Table 2. Copolymer PDMS10K-IP-B2, which has larger average segmental lengths, shows a higher surface concentration of PDMS in three takeoff angles, while the difference between results from the fourth takeoff angle is less than the experimental uncertainty. These data indicate that for copolymers with similar bulk compositions, the thickness of the phase-separated regions at the surface is influenced by the length of the low surface energy soft block. To understand the significance of the two comparisons described above, proper consideration must be given to the fact that the composition of the hard segments changes with the length. Therefore, in addition to phase separation due to the favorable entropic effect of longer soft segments, of equal or greater importance is phase separation driven by the enthalpic effect of stronger hydrogen bonding of larger hard blocks. These two effects may act in a synergistic fashion. This topic will be explored further in a later section.

The molecular weight distributions for the eight samples are very different, with polydispersities ranging from 1.3 to 2.8. It is not clear from our study what effect polydispersity may have on surface properties.

Annealing Effects. The surface compositions of PDMS–PU copolymer samples after a short annealing, as measured by ESCA, are summarized in Table 3, and corresponding data for samples after a long annealing are listed in Table 4.[29]

For samples with the shortest PDMS segments (MW_{soft} = 1000), annealing does not have any detectable effect on the surface concentration of PDMS. For samples with PDMS segments of moderate length (MW_{soft} = 2.4K), the only increase in PDMS surface concentration was observed in the sample with the longest hard segments. An annealing of 15 min at 120 °C was sufficient to cause the observed change. If the PDMS segments are long (MW_{soft} = 10K), significant changes in the PDMS surface concentrations are observed regardless of the composition of the hard segment. For example, the concentration of PDMS in the as-cast films of PDMS10K-IP-B0 and PDMS10K-IP-B2 measured at the lowest takeoff angle are 98.9 and 97.7%, respectively; after annealing, the corresponding values are 99.9 and 99.4%. The dominance of PDMS segments in the surface region is even more pronounced in copolymer PDMS27K-IP-B2. No hard segments were detected in measurements taken at the lowest takeoff

Table 3. PDMS Weight Percent of the Copolymer Samples, Annealed at 120 °C for 15 min

no.	sample ID	PDMS wt % $\theta = 10°$	$\theta = 15°$	$\theta = 30°$	$\theta = 90°$	bulk
1	PDMS1K-IP-B0	93.7 ± 0.2	90.8 ± 0.8	87.3 ± 0.5	84.0 ± 0.6	79.0
2	PDMS1K-IP-B0.5	88.6 ± 2.2	81.9 ± 1.6	75.2 ± 0.6	69.7 ± 0.4	68.8
3	PDMS2.4K-IP-B0	97.1 ± 0.5	95.4 ± 1.0	92.5 ± 0.4	91.3 ± 0.4	90.3
4	PDMS2.4K-IP-B1	94.8 ± 1.3	91.9 ± 0.8	85.4 ± 0.5	81.2 ± 0.4	79.4
5	PDMS2.4K-IP-B2	93.6 ± 1.8	89.5 ± 0.3	79.8 ± 0.2	74.1 ± 0.3	70.8
6	PDMS10K-IP-B0	99.9 ± 0.1	99.5 ± 0.2	98.5 ± 0.7	97.1 ± 0.2	97.5
7	PDMS10K-IP-B2	99.4 ± 0.8	98.5 ± 0.2	96.2 ± 1.9	93.2 ± 1.0	91.1
8	PDMS27K-IP-B2	100 ± 0.0	99.9 ± 0.0	99.1 ± 0.1	97.6 ± 0.2	96.5

Table 4. PDMS Weight Percent of the Copolymer Samples, Annealed at 120 °C for 2 h

sample no.	sample ID	PDMS wt % $\theta = 10°$	$\theta = 15°$	$\theta = 30°$	$\theta = 90°$	$\theta = 90°$ [a]	bulk
1	PDMS1K-IP-B0	91.9 ± 2.1	91.2 ± 0.9	86.5 ± 0.3	86.5 ± 0.3	83.7 ± 1.2	79.0
2	PDMS1K-IP-B0	89.1 ± 2.0	88.7 ± 6.5	80.3 ± 0.4	73.6 ± 0.2	72.5 ± 1.2	68.8
3	PDMS2.4K-IP-B0	98.5 ± 1.2	98.4 ± 0.8	94.3 ± 0.1	91.9 ± 1.1	89.2 ± 1.1	90.3
4	PDMS2.4K-IP-B1	93.1 ± 1.8	91.6 ± 0.2	87.4 ± 2.0	80.3 ± 0.7	79.1 ± 0.5	79.4
5	PDMS2.4K-IP-B2	94.2 ± 4.5	92.7 ± 2.4	80.0 ± 0.8	73.1 ± 2.1	69.2 ± 0.4	70.8
6	PDMS10K-IP-B0	100 ± 0.0	100 ± 0.0	99.1 ± 0.1	98.5 ± 0.4	97.6 ± 0.2	97.5
7	PDMS10K-IP-B2	100 ± 0.0	99.3 ± 0.2	97.2 ± 1.2	91.4 ± 0.9	89.0 ± 4.2	91.1
8	PDMS27K-IP-B2	100 ± 0.0	100 ± 0.0	98.9 ± 0.7	97.6 ± 0.4	87.0 ± 1.8	96.5

[a] With Ti anode X-ray source.

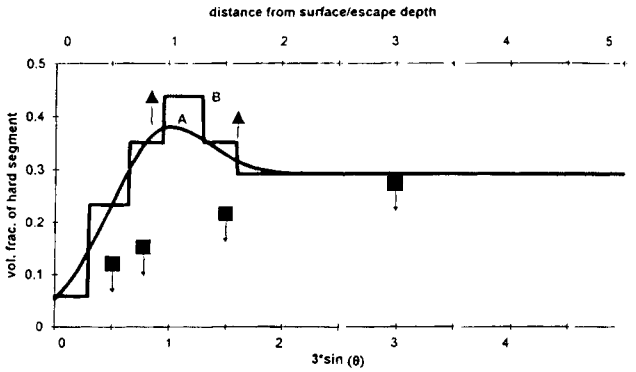

Figure 2. Concentration–depth profiles for the hard segment in as-cast films of copolymer PDMS2.4K-IP-B2. Profiles: (A) constructed based on a continuous model; (B) constructed based on a discrete model; (■) data measured by ESCA.

angle. The maximum sampling depth in ESCA measurements using a Ti anode is estimated to be 210 Å, which is about twice the maximum sampling depth attainable with a Mg anode. By using a Ti anode, the composition over a larger span of polymer surface can be evaluated. In Table 4, surface compositions of the films after a long annealing are listed, including results from a sampling depth at 210 Å. A continuous decrease in the concentration of PDMS in the surface region was observed.

Segmental Concentration–Depth Profile. Depth profiles for the hard segment in each copolymer have been recovered, and the profiles reveal some features that are not obvious in the ESCA data. In the following, the depth profile for the hard segment in copolymer PDMS2.4K-IP-B2 is used as a representative result to illustrate these features. In Figure 2, curve A represents the profile calculated by the continuous model, and curve B the profile calculated the discrete model. The curves were generated on the basis of experimental data and parameters listed in Tables 5–7. The keys to read these tables are contained in Table 8. Experimental ESCA data are plotted as a function of the sampling depth in the same figure as a contrast. Both models indicate a maximum in the profile, which is not readily discernible from the experimental ESCA data. This

Table 5. Concentration–Depth Profile Data for Copolymer PDMS2.4K-IP-B2 before Annealing

takeoff angle (deg)	10	15	30	90
upper uncertainty limit	37.4	29.0	20.5	16.2
C/N (ESCA data)	32.2	26.2	19.3	15.7
lower uncertainty limit	28.4	24.0	18.2	15.3
C/N (discrete model)	36.0	27.6	19.1	15.4
C/N (continuous model)	32.6	26.2	19.1	15.8

1. Parameters for the Depth Profile of the Hard Segment for the Discrete Model

δ_1	δ_2	$v(\infty)$	h_1	h_2	h_3	h_4	h_5	h_6	h_7	h_8
0.30	0.35	0.292	0.2	0.8	1.2	1.5	1.2	1.0	1.0	1.0

2. Parameters for the Depth Profile of the Hard Segment for the Continuous Model

y_1	l_1	σ_1	σ_2
1.30	1.00	0.50	0.38

Table 6. Concentration–Depth Profile Data for Copolymer PDMS2.4K-IP-B2, Annealed at 120 °C for 15 min

takeoff angle (deg)	10	15	30	90
upper uncertainty limit	79.2	37.4	20.5	16.7
C/N (ESCA data)	57.8	36.4	20.3	16.5
lower uncertainty limit	45.7	35.4	20.2	16.4
C/N (discrete model)	55.4	36.6	20.5	14.9
C/N (continuous model)	55.6	36.9	20.4	14.6

1. Parameters for the Depth Profile of the Hard Segment for the Discrete Model

δ_1	δ_2	$v(\infty)$	h_1	h_2	h_3	h_4	h_5	h_6	h_7	h_8
0.31	0.35	0.292	0.1	0.6	1.2	1.8	1.9	1.5	1.1	1.0

2. Parameters for the Depth Profile of the Hard Segment for the Continuous Model

y_1	l_1	σ_1	σ_2
1.99	1.30	0.50	0.48

underlines the fact that for polymers with partially or completely phase separated surface regions, the convoluted nature of the photoelectron intensity signals prevents a direct measurement of concentration–depth profiles. Profiles suggested by both models, when inserted into the convolution equations, lead to photoelectron intensity ratios in very good agreement with

Table 7. Concentration–Depth Profile Data for Copolymer PDMS2.4K-IP-B2, Annealed at 120 °C for 2 h

takeoff angle (deg)	10	15	30	90
upper uncertainty limit	272.6	74.5	21.3	17.1
C/N (ESCA data)	63.4	51.0	20.5	16.0
lower uncertainty limit	37.0	39.1	19.8	15.1
C/N (discrete model)	97.0	47.2	22.7	16.0
C/N (continuous model)	61.2	40.4	21.9	15.3

1. Parameters for the Depth Profile of the Hard Segment for the Discrete Model

δ_1	δ_2	$v(\infty)$	h_1	h_2	h_3	h_4	h_5	h_6	h_7	h_8
0.34	0.35	0.292	0	0.7	1.3	1.8	1.4	1.1	1.0	1.0

2. Parameters for the Depth Profile of the Hard Segment for the Continuous Model

y_1	l_1	σ_1	σ_2
1.82	1.30	0.50	0.64

experimental data as shown in Table 5. The effects of annealing on depth profiles are shown in Figure 3 (based on the discrete model) and in Figure 4 (based on the continuous model). Both models reveal increases in the thickness of PDMS and hard-block-enriched phases after annealing. The thickness of the topmost PDMS layer with less than 5% hard segment content increases from zero to 0.2λ (about 0.7 nm). The thickness of the layer enriched with hard segments, which is responsible for the maximum in the profile, doubles, in this case, from $\sim\lambda$ to $\sim 2\lambda$. These observations again illustrate the positive effects of annealing in enhancing the surface concentration of PDMS.

Effects of different λ_C to λ_N ratios on the shape of the deconvoluted depth profile for the hard segment in copolymer PDMS2.4KK-IP-B2 are illustrated in Figure 5. Curve A was obtained with λ_C equal to λ_N, and for curve B λ_C equals 1.1 times λ_N. We do not know the true ratio of λ_C to λ_N to any precision beyond that it falls between 1 and 1.1. The assumption used in this work was λ_C equals λ_N. Had the assumption been λ_C is 1.1 times λ_N, a slightly different depth profile would result. The location of the maximum hard segment concentration and the shape of the shoulder to the left of the maximum vary little; the height of the peak increases and the shoulder to the right of the maximum broadens. These differences do not affect the conclusions reached in this work regarding the distribution of the various components and the effects of annealing on that distribution. Both assumptions on the λ ratio lead to depth profiles characterized by a hard-segment-deficient top surface and an adjacent hard-segment-enriched layer. Annealing, as shown in Figure 4, has very strong effects on the location of the peak; different assumptions on λ's do not mask those effects.

Effects of Structure and Molecular Weight on the Distribution of the Hard Segment. In addition to the difference in surface energies, which is the underlying driving force for the enrichment of PDMS segments at the surface, there are two additional factors that contribute to the observed surface phase separation. Long soft segments amplify entropically driven phase separation, and increased hydrogen bonding in hard segments augments the enthalpic driving force for phase separation. The interplay of these factors under different situations is discussed below.

We define $v_N(x)$ as

$$v_N(x) = \{v(x)/[1 - v(x)]\}/\{v(\infty)/[1 - v(\infty)]\} \quad (15)$$

Equation 15 represents the normalization of the volume fraction of the hard segment at the surface region, $v(x)$, with respect to the bulk value, $v(\infty)$. The quantity $v_N(x)$ can also be visualized in the following way. Suppose a unit volume of soft segments with the entrapped hard segments moves from the bulk (location ∞) to the surface (location x), and during the movement the hard segments gradually drop out this volume due to the progress of phase separation, then $v_N(x)$ represents the fraction of the initial hard segments remaining at the end of the movement. Using this measurement, materials can be compared on the basis of their "effectiveness" in separating the soft and the hard segments.

In Figure 6, v_N depth profiles for copolymers PDMS10K-IP-B0 (A, C) and PDMS10K-IP-B2 (B, D) are shown. The curves are for films as-cast and after an annealing at 120 °C for 15 min. These curves are similar to those for PDMS2.4K-IP-B2 described earlier. There is a hard-segment-enriched region beneath the

Table 8. Keys To Read Concentration–Depth Profile Data

C/N (ESCA data): the average of three measurements
upper uncertainty limit: the average plus one standard deviation based on three measurements
lower uncertainty limit: the average minus one standard deviation based on three measurements
C/N (discrete model): calculated from the discrete model (see text for details of this model) with the optimal parameters
C/N (continuous model): calculated from the continuous model (see text for details of this model) with the optimal parameters

Parameters for the Discrete Model

The depth profile is described with a series of 11 numbers. These numbers are used to specify the starting position and height of each constituent step function. (Refer to profiles in Figure 2 for illustration.) The first two numbers are the staggered distances between the two step functions. In this study, the distances staggered were kept alternating between two values. For example, the staggered distances between two consecutive step functions for the profile shown in Figure 2 are 0.30λ and 0.35λ, alternately. The third number is the bulk value for the volume fraction of the hard segment, which is also equal to the sum of the heights of all the nine step functions. The forth number is the height of the first step function; the fifth number is the sum of the heights of the first and the second step functions. Similarly, each subsequent number is the sum of the previous number and the height of an additional step function. (From the forth to the eleventh number, the value is normalized with respect to the bulk volume fraction, i.e. the third number.)

Parameters for the Continuous Model

The depth profile is described with a four-parameter compound Gaussian distribution model of the form

$$y(l) = y_1 \exp[-0.5(l - l_1)^2/\sigma_1^2] \quad l \le l_1$$
$$= 1 + (y_1 - 1) \exp[-0.5(l - l_1)^2/\sigma_2^2] \quad l > l_1$$

where y is $v(l)/v(\infty)$, $v(\infty)$ the bulk value of v, the volume fraction of the hard segment; l is the distance from the surface divided by the escape depth. The four parameters are y_1, the maximum y value of the profile; l_1, the location of the maximum of the profile; and σ_1 and σ_2 which characterize the shape of the profile to the left and to the right of the maximum, respectively.

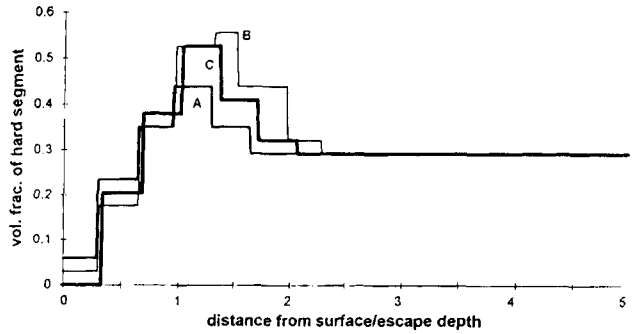

Figure 3. Concentration–depth profiles of the hard segments in the surface region for the copolymer PDMS2.4K-IP-B2 under different thermal treatments. The profiles are constructed on the basis of a discrete model. Curves: (A) as-cast; (B) annealed at 120 °C for 15 min; (C) annealed at 120 °C for 2 h.

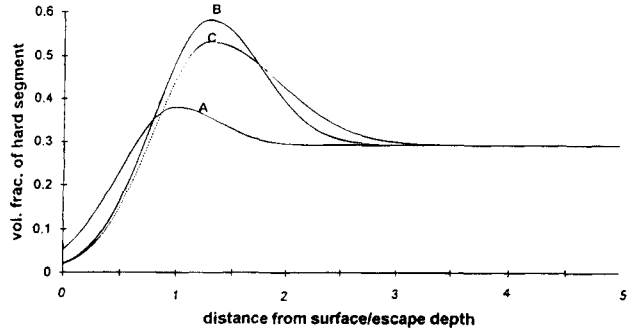

Figure 4. Concentration–depth profiles of the hard segments in the surface region for the copolymer PDMS2.4K-IP-B2 under different thermal treatments. The profiles are constructed on the basis of a continuous model. Curves: (A) as-cast; (B) annealed at 120 °C for 15 min; (C) annealed at 120 °C for 2 h.

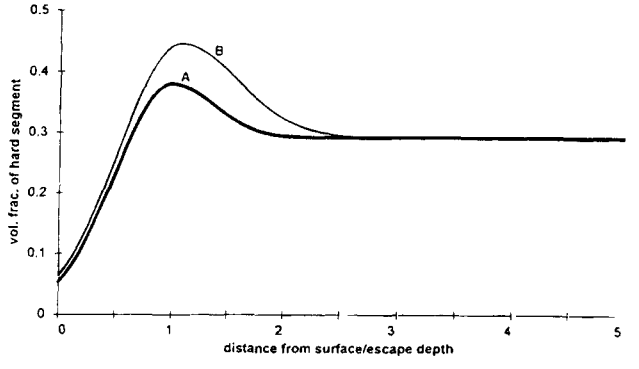

Figure 5. Effects of different λ_C to λ_N ratios on the shape of the deconvoluted depth profile for the hard segment in copolymer PDMS2.4K-IP-B2. Curve A was obtained with λ_C equal to λ_N, and curve B with λ_C equal to 1.1 times λ_N.

hard-segment-deficient surface layer, and annealing increases the thickness of both layers. In this section we will focus on the lower left corner of Figure 6 representing the region less than one λ (ca. 3.4 nm) from the surface. That portion is enlarged and roplotted in Figure 7. The two solid curves (A, B), representing concentration profiles in the as-cast films, indicate that the incorporation of chain extender promotes surface phase separation at ambient temperature presumably due to the increased interactions among the hard segments. This advantage is lost in annealing as both after-annealing profiles (dashed curves) are similar and shift to lower hard segment concentrations. Since the soft segments are the same and relatively large compared to the hard segments, the occurrence of the

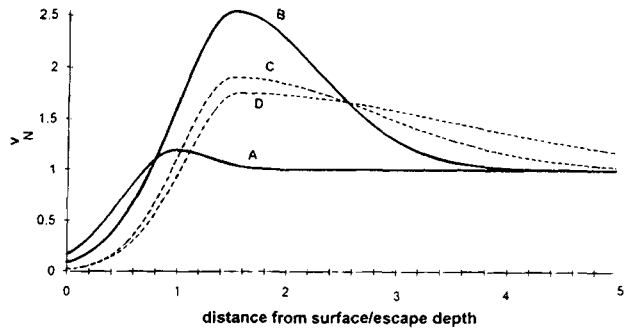

Figure 6. v_N as a function of depth in the surface region for two copolymers. Curves: (A) PDMS10K-IP-B0 as-cast; (B) PDMS10K-IP-B2 as-cast; (C) PDMS10K-IP-B0 annealed at 120 °C for 15 min; (D) PDMS10K-IP-B2 annealed at 120 °C for 15 min.

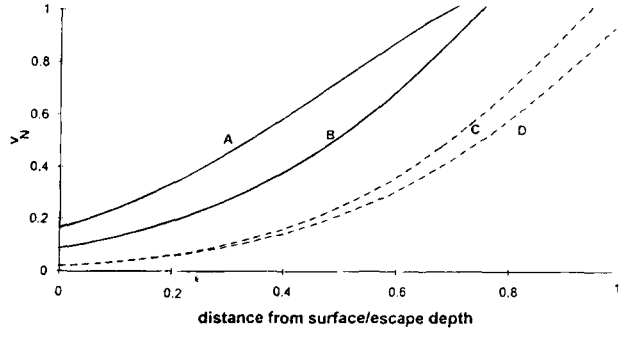

Figure 7. v_N as a function of depth in the topmost surface region for two copolymers. Curves: (A) PDMS10K-IP-B0 as-cast; (B) PDMS10K-IP-B2 as-cast; (C) PDMS10K-IP-B0 annealed at 120 °C for 15 min; (D) PDMS10K-IP-B2 annealed at 120 °C for 15 min.

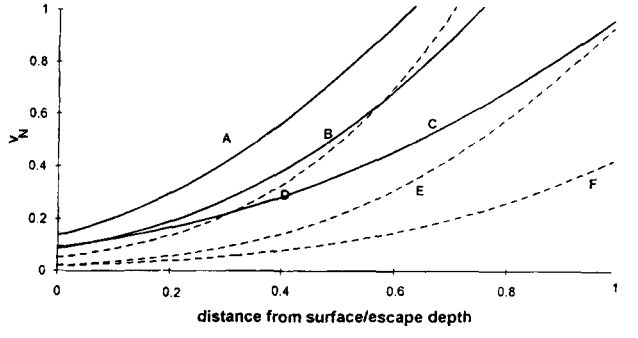

Figure 8. v_N as a function of depth in the topmost surface region for three copolymers. Curves: (A) PDMS2.4K-IP-B2 as-cast; (B) PDMS10K-IP-B2 as-cast; (C) PDMS27K-IP-B2 as-cast; (D) PDMS2.4K-IP-B2 annealed at 120 °C for 15 min; (E) PDMS10K-IP-B2 annealed at 120 °C for 15 min; (F) PDMS27K-IP-B2 annealed at 120 °C for 15 min.

similar near-surface profiles after short annealing is driven by enthalpy. Thus, the rate of disadvantaged phase separation for PDMS10K-IP-B0 catches up to that of PDMS10K-IP-B2, as an increase in temperature enhances the higher-energy-barrier phase separation process for PDMS10K-IP-B0.

In Figure 8, v_N profiles for copolymers PDMS2.4K-IP-B2, PDMS10K-IP-B2, and PDMS27K-IP-B2 are plotted. Cast at ambient temperature, the hard segment concentration in the surface region decreases with an increase in the average molecular weight of the soft segments. After annealing, the curves shift to lower hard segment concentrations while the relative positions to one another are maintained. The inverse correlation between surface hard segment concentration and bulk soft segment molecular weight as well as the insensitiv-

ity of the shape of the curve to temperature points to entropic origins for the observed differences.

Conclusions

We have investigated the effects of segmental length and annealing on the surface composition of films of segmented poly(dimethylsiloxane–urea–urethane)s. The films were cast from solutions in THF, a mutual solvent for the hard and soft segments. In general, the surface concentration of PDMS increases with the length of that segment. As the PDMS segmental molecular weight reaches 27 000, ESCA data indicate that the topmost surface region of the as-cast films of the copolymer is composed of nearly 100% PDMS.

Annealing the as-cast samples increases the PDMS concentration in the topmost region. Thus, the surface of annealed copolymers (120 °C for 15 min) with a 10K PDMS segmental molecular weight consists of almost pure PDMS.

Segmental depth profiles were constructed from ESCA data. The profile typically contains a maximum and can be described by either a summation of step functions or a compound Gaussian distribution. The existence of a maximum indicates a PDMS-deficient region beneath the PDMS-enriched region. Annealing increases the thickness of both regions.

It has been demonstrated that both the length of the soft segments and the interactions among the hard segments affect the phase separation in the surface region. Long soft segments amplify entropically driven phase separation, and increased hydrogen bonding in hard segments augments the enthalpic driving force for phase separation.

Acknowledgment. This research was supported in part by the Office of Naval Research.

References and Notes

(1) Brady, R. F.; Griffith, J. R.; Love, K. S.; Field, D. E. *J. Coat. Technol.* **1987**, *59*, 113.
(2) Ho, T.; Wynne, K. J. *Macromolecules* **1992**, *25*, 3521.
(3) McCarthy, T.; Ho, T.; Wynne, K. J. Unpublished results.
(4) Ho, T.; Wynne, K. J.; Nissan, R. *Macromolecules* **1993**, *26*, 7029.
(5) Patel, N. M.; Dwight, D. W.; Hedrick, J. L.; Webster, D. C.; McGrath, J. E. *Macromolecules* **1988**, *21*, 2689.
(6) Smith, S. D.; DeSimone, J. M.; Huang, H.; York, G.; Dwight, D. W.; Wilkes, G. L.; McGrath, J. E. *Macromolecules* **1992**, *25*, 2575.
(7) Chen, X.; Gardella, J. A., Jr. *Polym. Prepr. (Am. Chem. Soc., Div. Polym. Chem.)* **1992**, *33* (2), 312.
(8) Chen, X.; Gardella, J. A., Jr.; Kumler, P. L. *Macromolecules* **1993**, *26*, 3778.
(9) Schmitt, R. L.; Gardella, J. A., Jr.; Magill, J. H.; Salvati, L., Jr.; Chin, R. L. *Macromolecules* **1985**, *18*, 2675.
(10) Mittlefehldt, E. R.; Gardella, J. A., Jr. *Appl. Spectrosc.* **1989**, *43*, 1172.
(11) Chen, X.; Lee, H. F.; Gardella, J. A., Jr. *Macromolecules* **1993**, *26*, 4601.
(12) Clark, D. T.; Peeling, J.; O'Malley, J. M. *J. Polym. Sci., Polym. Chem. Ed.* **1976**, *9*, 879.
(13) Chen, X.; Gardella, J. A., Jr.; Kumler, P. L. *Macromolecules* **1992**, *25*, 6621.
(14) Chen, X.; Gardella, J. A., Jr.; Kumler, P. L. *Macromolecules* **1992**, *25*, 6631.
(15) Thomas, H. R.; O'Malley, J. J. *Macromolecules* **1979**, *12*, 323.
(16) Coulon, G.; Russell, T. R.; Deline, V. R.; Green, P. F. *Macromolecules* **1989**, *22*, 2581.
(17) Clark, D. T. *Adv. Polym. Sci.* **1977**, *24*, 126.
(18) Pijolat, M.; Hollinger, G. *Surf. Sci.* **1981**, *105*, 114.
(19) Iwasaki, H.; Nishitani, R.; Nakamura, S. *Jpn. J. Appl. Phys.* **1978**, *17*, 1519.
(20) Holloway, P. H.; Bussing, T. D. *Surf. Interface Anal.* **1992**, *18*, 251.
(21) Nefedov, V. I.; Baschenko, O. A. *J. Electron Spectrosc. Relat. Phenom.* **1988**, *47*, 1.
(22) Tyler, B. J.; Castner, D. G.; Ratner, B. D. *Surf. Interface Anal.* **1989**, *14*, 443.
(23) Jisl, R. *Surf. Interface Anal.* **1990**, *15*, 719.
(24) Vargo, T. G.; Gardella, J. A., Jr. *J. Vac. Sci. Technol.* **1989**, *A7*, 1733.
(25) Seah, M. P.; Dench, W. A. *Surf. Interface Anal.* **1979**, *1*, 2.
(26) Chen, X.; Gardella, J. A., Jr.; Cohen, R. E. *Macromolecules* **1994**, *27*, 2206.
(27) Seinfeld, J. H.; Lapidus, L. *Mathematical Methods in Chemical Engineering, v.3 Process Modeling, Estimation, and Identification*; Prentice-Hall, Inc.: Englewood Cliffs, NJ, 1974; p 383.
(28) Wu, S. *Polymer Interface and Adhesion*; Marcel Dekker: New York, 1982; p 184.
(29) In a companion study by GPC, it was found that annealing at 120 °C for 2 h has insignificant effects on the average molecular weights of the current copolymers.

MA941297M